Original Research

Copper-Doped Zinc Oxide Nanoparticles: An Eco-Benign Synthesis, Photocatalytic and Antimicrobial Activities

Naveed Ahmad [1], Muhammad Saleem [1], Munawar Iqbal [2,3], Mazhar Abbas [4], Ismat Bibi [5], Aljawhara H. Almuqrin [6], Nissren Tamam [6], Manar S. Alshatwi [6], Arif Nazir [7], Norah Alwadai [6,*]

[1] Department of Chemistry, Minhaj University, Lahore, Pakistan
[2] Renewable Energy and Environmental Technology Center, University of Tabuk, Tabuk, 47913, Saudi Arabia
[3] School of Chemistry, University of the Punjab, Lahore 54590, Pakistan
[4] Department of Basic Sciences (Section Biochemistry), University of Veterinary and Animal Sciences Lahore (Jhang Campus), Jhang, Pakistan
[5] Institute of Chemistry, The Islamia University of Bahawalpur, Bahawalpur, Pakistan
[6] Department of Physics, College of Sciences, Princess Nourah bint Abdulrahman University, P.O. Box 84428, Riyadh 11671, Saudi Arabia
[7] Department of Chemistry, The University of Lahore, Lahore, Pakistan
* Correspondence: nmalwadai@pnu.edu.sa

Received: December 12, 2025; Accepted: April 29, 2026

Abstract: Copper-doped zinc oxide nanoparticles (Cu-d-ZnO NPs) were prepared via a precipitation-dispersion method with different copper concentrations (1–5%) and the structural, photocatalytic and antimicrobial properties were studied. XRD analysis revealed that ZnO has a hexagonal structure with a decrease in particle size with increasing copper content. The average crystallite sizes were found to be 27.8±2.0 nm, 24.6±1.6 nm and 21.9±1.7 nm for 1%, 3% and 5% Cu-doped ZnO samples, respectively. The morphology analysis revealed a porous structure with cluster aggregate formation of the NPs and EDX analysis revealed the presence of Zn, Cu and O elements. Thermal analysis revealed that ZnO NPs have good thermal stability up to 900 °C with 9.16-29.31% mass loss. Photocatalytic activity against methylene blue (MB) dye was carried out under UV light irradiation and it was found that 85.5% removal was achieved for Cu (5%)-d-ZnO NPs, whereas ZnO furnished 58% efficiency. Results of the antimicrobial study against *S. aureus, B. subtilis, E. coli* and *P. multocida* indicated 30% enhanced activity of Cu-d-ZnO as compared to pure ZnO. The minimum inhibitory concentration of Cu-d-ZnO against bacteria was found to be 178–354 μg/mL, whereas against fungi (*A. flavus*, *A. niger* and *P. notatum*), the values of the minimum inhibitory concentration of Cu-d-ZnO were found to be 286–407 μg/mL. Scavenger studies revealed that photogenerated electrons play a crucial role in initiating reactive oxygen species formation through reduction of dissolved oxygen to superoxide radicals ($O_2^{\bullet-}$), while hydroxyl radicals ($^{\bullet}OH$), generated via hole-mediated oxidation of water and hydroxyl ions, act as the primary oxidizing species responsible for dye degradation. These findings demonstrate that Cu doping enhances charge separation and reactive oxygen species generation, thereby improving photocatalytic efficiency. These results indicate the potential of Cu-d-ZnO NP to be used for the remediation of dyes as well as for the treatment of infections. The Cu-d-ZnO NPs show strong potential for applications in dye remediation and antimicrobial treatment. Future work should focus on optimizing operational parameters and evaluating toxicity and environmental safety for practical applications.

Keywords: Copper-doped ZnO; Precipitation-dispersion; Photocatalytic degradation; Methylene blue; Antimicrobial activity

1. Introduction

Nanotechnology has achieved importance in all fields of life. The NPs have been successfully applied in the biomedical fields. The NPs offered unique properties versus bulk material. The properties changed many folds with the reduction of the size of materials to nm [1-3]. To date, various approaches are in practice to enhance the properties (physicochemical) of metal oxide NPs for applications in different fields [4]. The ZnO has a wide range of applications in solar energy transformation, electronics, catalysis, biomedical and adsorbent etc. ZnO is a more excellent UV-emitting material than GaN (Gallium Nitride) due to its exciton binding energy. The ZnO properties can be enhanced by doping and resultantly, the properties can be tailored via quantum confinement and surface effects, which can be achieved by metal ion doping [5]. ZnO is used because it is inexpensive, non-toxic, and abundant in nature and also offers optical transparency in the entire range and most importantly, is useful in doping. Such a doped material is expected to have promising applications in electronic and optoelectronic devices [6, 7].

The doped ZnO has been studied using different synthesis approaches, each of which has a major impact on their structural, optical and functional characteristics. For Gd-, Fe- and Co-doped ZnO, hydrothermal techniques are widely used because they can yield materials with lower band gaps, increased surface area and improved photo-reactivity, which make them appropriate for gas sensing and photoelectrochemical applications. While magnetron sputtering allows Ta-doped ZnO with smaller particles and defect engineering for sensing applications, combustion synthesis has been used for (Al, Ga)-doped ZnO to enhance the electrical conductivity and thermoelectric performance. On the other hand, the sol-gel route, as demonstrated for Ce-doped ZnO, provides efficient control over microstructure, morphology and conductivity, while being relatively straightforward and scalable [8-14]. Nevertheless, a large number of the adopted techniques suffer from a lack of scalability or overly complicated methodologies. Thus, the precipitation-dispersion approach to Cu-d-ZnO in the present work provides a simple yet cost-effective approach to the precise incorporation of dopants, structural tailoring, as well as enhanced functional properties [15].

Despite the extensive research carried out on metal-doped ZnO nanomaterials, most of the research has focused on either photocatalysis or antibacterial activity, with little emphasis given to the effect of dopant concentration on the simultaneous multifunctional properties [16, 17]. Furthermore, there are still a few systematic studies and their effects on particle size, thermal stability, dye degradation efficiency and minimum inhibitory concentrations. By preparing Cu-d-ZnO NPs (1–5%) and establishing a direct structure–property relationship through thorough characterization and application studies, the current work fills this gap. The current work aims to synthesize Cu-d-ZnO NPs using a precipitation–dispersion route with controlled Cu loadings (1–5%) and to establish a structure–property–activity relationship in light of the aforementioned considerations and the paucity of systematic studies correlating copper dopant concentration with multifunctional performance. XRD, SEM, TGA and EDX techniques were employed for characterizing Cu-d-ZnO. The photocatalytic activity was evaluated by degrading MB dye (Fig. 1) under UB light irradiation, while the antimicrobial activity was studied against microbial (*P. multocida, B. subtilis, S. aureus* and *E. coli*) and fungal strains (*A. niger, P. notatum* and *A. flavus*).

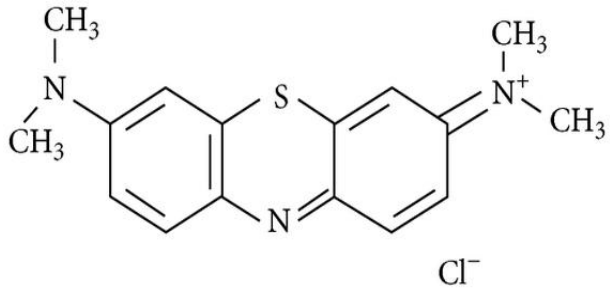

Figure 1. Chemical structure of methylene blue (MB) dye used as a model pollutant in photocatalytic degradation experiments.

2. Material and methods

2.1. Materials

The zinc oxide (ZnO, ≥99.5%), copper sulfate pentahydrate ($CuSO_4{\cdot}5H_2O$, ≥99%), sodium hydroxide (NaOH, ≥98%), citric acid (≥99.5%), ammonia solution (25–28%), methylene blue (≥98%), hydrochloric acid (HCl, 37%), rifampicin (≥97%), fluconazole (≥98%) and ethanol were supplied by Sigma-Aldrich (Germany). Oxoid (UK) provided the potato dextrose broth and nutrient broth. All analytical-grade chemicals were used and all of the trials were conducted using distilled water.

2.2. Synthesis procedure

The Cu-d-ZnO NPs with 1, 3, and 5 wt.% Cu was synthesized using a precipitation–dispersion method. Initially, 20 mL of 0.1 *M* citric acid solution was prepared and an appropriate amount of $CuSO_4{\cdot}5H_2O$ was dissolved in the citric acid solution under continuous stirring. The resulting mixture was transferred to a 500 mL flask and maintained at 70 °C for 20 min. Subsequently, 1.0 g of ZnO powder was gradually added to the solution under constant stirring at 70 °C. Then, 2.0 mL of ammonia solution (NH_3) was added dropwise (pH ~8.2). The reaction mixture was then stirred at 70 °C for 3 h. Then, the suspension was allowed to cool to 25 °C and was separated by centrifugation at 5000 rpm for 10 min. The obtained precipitate was washed several times with distilled water and ethanol to remove unreacted species and residual impurities. Finally, the product was dried at 70 °C for 24 h and calcined at 750 °C for 4 h.

2.3. Photocatalytic activity (PCA)

MB was used to assess the photocatalytic activity of pristine ZnO and Cu-d-ZnO NPs (Cu 1, 3, and 5 wt%) under UV irradiation. The catalyst (6 mg) was dispersed in the MB dye solution (50 mL, 10 mg/L) and stirred for 30 minutes in the dark. Then, the mixture was subjected to irradiation (high-pressure mercury vapor lamp, 400 W, having emission at 365 nm). To ensure uniform illumination, the lamp was placed 10 cm from the reactor. Using a UV radiometer, the light intensity at the solution surface was determined to be 18±2 mW cm^{-2}. Continuous stirring and external water circulation were used to keep the reaction temperature at 25±2 °C during irradiation. At different time intervals, 3 mL of the reaction mixture was withdrawn and filtered using a Millipore membrane filter to remove catalyst particles. The absorbance of the filtrate was measured at 664 nm using a UV–visible spectrophotometer (CE Cecil 7200, UK). The remaining concentration of MB dye was determined from the absorbance values and the degradation efficiency was calculated using Eq. 1 [19].

$$\text{Degradation (\%)} = \frac{C_0 - C_t}{C_0} \text{ x } 100 \qquad (1)$$

Where C_0 and C_t stand for MB's initial and time-dependent absorbance values, respectively. To enable direct comparison between ZnO and Cu-d-ZnO samples, all experiments were conducted under identical conditions. A triplicate sample was run for photocatalytic evaluation and the response was presented as mean ± standard deviation.

2.4. Antimicrobial activity

2.4.1. Microbial strains

The antibacterial and antifungal activities of Cu-d-ZnO NPs with varying Cu contents (1, 3 and 5 wt.%) were evaluated against selected microbial strains, including *P. multocida*, *B. subtilis*, *S. aureus*

and *E. coli* (bacteria) and *A niger*, *P. notatum* and *A. flavus* (fungi). The microbial strains were obtained from the Protein Molecular Laboratory (PML), University of Agriculture Faisalabad (UAF), Pakistan. Bacterial strains were cultured in nutrient broth (Oxoid, UK) at 37 °C for 24 h, while fungal strains were grown in potato dextrose broth (Oxoid, UK) at 28 °C for 72 h before antimicrobial testing.

2.4.2. Culture preparation

Fresh cultures of bacteria (nutrient broth, Oxoid, UK) and fungi (potato dextrose broth, Oxoid, UK) were maintained under aseptic conditions. Fresh cultures of bacteria (1×10^8 CFU/mL) were used for the study.

2.4.3. Disc diffusion method

The antimicrobial activity of Cu-d-ZnO NPs containing 1, 3, and 5 wt.% Cu was evaluated using the disc diffusion method. Potato dextrose agar (PDA) and nutrient agar (NA) were prepared in distilled water for fungal and bacterial cultures, respectively and sterilized by autoclaving at 121 °C for 15 min. Sterile filter paper discs (9 mm in diameter) were also prepared. 20 mL of sterilized agar medium (for antibacterial assays) and potato dextrose agar (for antifungal assays) was poured into sterile Petri plates and allowed to solidify in a laminar air flow. Each plate was then inoculated with fresh microbial culture to form a uniform bed. Sterile discs were impregnated with 100 μL of test samples, including Cu-d-ZnO NPs (1, 3, and 5 wt.% Cu), pure ZnO and standard drugs (rifampicin and fluconazole) and placed onto the surface of the inoculated agar medium (antibacterial assays) and potato dextrose agar (antifungal assays) plates using sterile forceps. The bacterial plates were incubated at 37 °C for 24 h, while fungal plates were incubated at 28 °C for 48 h. After incubation, the antimicrobial activity was assessed by measuring the diameter of the zones of inhibition (mm) using a zone reader [20].

2.4.4. MIC analysis

For the measurement of MIC, the serial dilution method is used. For this purpose, 100 μL of the sample is poured into the first row of a 96-well plate. Then, 50 μL of the sample is diluted in descending order. The sample is poured into the last well. Resazurin as an indicator (10 μL) is also added to each well. Finally, 10 μL of microorganism culture (5×10^6 CFU/mL) is also added to each well. This will result in a microorganism concentration of 5×10^5 CFU/mL in each well. Control (negative and positive) is also run in parallel. Plates are covered with aluminum foil and then incubated at 37°C for 24 h for bacterial growth and at 28°C for 48 h for fungal growth. Using a BioTek μ-Quant microplate reader (BioTek, Winooski, VT, USA), the absorbance was recorded at 500 nm. A color change from purple to pink or colorless is interpreted and the MIC value is determined by taking the lowest concentration at which a color change is observed.

The minimum inhibitory concentration (MIC) of Cu-d-ZnO NPs was determined using a standard broth microdilution method in a 96-well microplate. Briefly, 100 μL of the test sample was added to the first well, followed by two-fold serial dilutions using 50 μL aliquots to obtain a range of decreasing concentrations. Subsequently, 10 μL of resazurin solution was added to each well as a viability indicator. A microbial suspension (10 μL, 5×10^6 CFU/mL) was then inoculated into each well to achieve a final inoculum of approximately 5×10^5 CFU/mL per well. The positive standard (antibacterial and antifungal agents) and negative (sterile medium) controls were included. The microplates were covered and incubated at 37 °C for 24 h for bacterial strains and at 28 °C for 48 h for fungal strains. After incubation, absorbance was recorded at 500 nm using a BioTek μQuant microplate reader (BioTek, Winooski, VT, USA). Microbial growth was indicated by a color change of resazurin from purple to pink or colorless. The MIC was defined as the lowest concentration of the test sample that prevented this color change, indicating inhibition of microbial growth [21].

3. Results and discussion

3.1. Properties of the Cu-d-ZnO

The XRD patterns of Cu-d-ZnO NPs for different concentrations of Cu doping are shown in Fig. 2. The prominent diffraction peaks observed at 2θ values of 31.7°, 34.4°, 36.2°, 47.5° and 56.6° correspond to the (100), (002), (101), (102), and (110) planes of hexagonal wurtzite ZnO, respectively.

These diffraction peaks correspond to the standard diffraction pattern of ZnO (JCPDS card no. 36-1451). These diffraction peaks correspond to the ZnO wurtzite structure. For the 1 wt.% Cu-d-ZnO sample (Figure 2A), the diffraction peaks were relatively sharper. The crystallite size (D) was calculated using the Scherrer equation (Eq. 2) [6].

$$D = \frac{0.9\lambda}{\beta\cos} \qquad (2)$$

where λ is 1.54 nm, β is the full width at half maxima and θ is Bragg's angle. To ensure reliability, the crystallite size was calculated from the diffraction peaks corresponding to the (100), (002) and (101) planes and the results were expressed as average values with standard deviation. The average crystallite sizes were found to be 27.8±2.0 nm, 24.6±1.6 nm and 21.9±1.7 nm for 1%, 3% and 5% Cu-doped ZnO samples, respectively. The observed reduction in crystallite size with increasing Cu concentration is attributed to lattice distortion and inhibition of crystal growth caused by Cu incorporation into the ZnO lattice. The XRD pattern of the 3 wt.% Cu-d-ZnO sample is depicted in Figure 2B. The characteristic diffraction peaks of ZnO were observed in the sample. This indicates that the wurtzite ZnO lattice structure is preserved during the doping of the Cu dopant. Slight peak shifts and broadening are observed, which may be due to the strain and distortion introduced during the substitution of Zn^{2+} (0.74Å) by Cu^{2+} (0.73Å) ions. In the case of the 5 wt.% Cu-doped sample, as depicted in Figure 2C, additional weak diffraction peaks are observed at a 2θ range of 28–33°, apart from the other minor diffraction peaks. This may be due to the Cu-related oxide species present as impurities, which is an indication that the high dopant concentration is affecting the material. From the XRD patterns, it is clear that the major phase present in the synthesized materials is the hexagonal wurtzite structure of ZnO, though there is a slight distortion due to the incorporation of Cu [15].

The surface morphology of the Cu-doped ZnO nanoparticles was examined using SEM (Figure 3A–C). All samples exhibit highly agglomerated structures composed of nearly spherical nanoparticles, which is a typical feature of ZnO-based nanomaterials due to their high surface energy and strong interparticle interactions. The particles appear densely packed, forming irregular clusters with rough surface texture. For the 1 wt.% Cu-doped ZnO sample (Figure 3A), relatively larger agglomerates are observed, indicating strong particle–particle adhesion. Upon increasing the Cu content to 3 wt.% (Figure 3B), the morphology becomes comparatively finer and more uniformly distributed, although agglomeration is still evident. In the 5 wt.% Cu-doped sample (Figure 3C), dense and highly aggregated clusters reappear, which may be attributed to enhanced interparticle interactions and possible defect-induced attraction at higher dopant concentration. Due to the pronounced agglomeration observed in all samples, reliable particle size measurement, size distribution analysis (histogram), and average particle diameter could not be accurately determined from SEM images alone. Therefore, SEM analysis is primarily used here to describe surface morphology rather than quantitative particle sizing. The nanoscale nature of the particles is instead confirmed by XRD analysis, where the crystallite sizes were calculated to be in the nanometer range. This indicates that the primary particles are nanosized, while SEM reveals their tendency to form larger agglomerated clusters.

The TGA and DSC profiles of the samples are presented in Figure 4, where the blue curves represent weight loss (TGA) and the green curves correspond to heat flow (DSC). The samples exhibit an initial minor weight loss below ~150 °C, which is attributed to the removal of physically adsorbed moisture and residual solvents. This step is accompanied by a weak endothermic signal in the DSC curves, confirming dehydration of surface-bound species. A second weight-loss region is observed between ~200 and 500 °C, corresponding to the decomposition of residual organic species and precursor-derived intermediates. The associated thermal events in the DSC curves (notably around 350–450 °C) further support the elimination of these organic components and the progressive purification of the material. Beyond 500 °C, the TGA curves show negligible weight change, indicating the formation of a thermally stable oxide framework. The DSC curves display broad exothermic features in the range of 600–800 °C, which are attributed to structural rearrangement, defect reduction, and lattice stabilization of the pre-formed ZnO phase rather than crystallization.

Since ZnO is already present before calcination, these thermal events are more reasonably associated with improved crystallinity and removal of residual defects or trace organics. The absence of significant mass loss above ~800 °C confirms the high thermal stability of the synthesized nanoparticles. Overall, the TG–DSC analysis indicates that most volatile and organic residues are removed below 500 °C, while higher temperatures promote structural ordering and stabilization of the ZnO lattice.

The elemental composition of the Cu-doped ZnO nanoparticles was analyzed using energy-dispersive X-ray (EDX) spectroscopy and a representative spectrum is shown in Figure 5. The spectrum exhibits prominent peaks corresponding to Zn and O, confirming the formation of ZnO as the primary phase. The presence of Cu is also detected, indicating successful incorporation of the dopant into the ZnO matrix. The intensity of the Cu signal increases with increasing dopant concentration (1–5 wt.%). A carbon peak is also observed, which is attributed to the carbon tape used during sample preparation. It is important to note that EDX is a semi-quantitative technique; therefore, the obtained elemental percentages provide only an approximate estimation of composition rather than precise stoichiometric values.

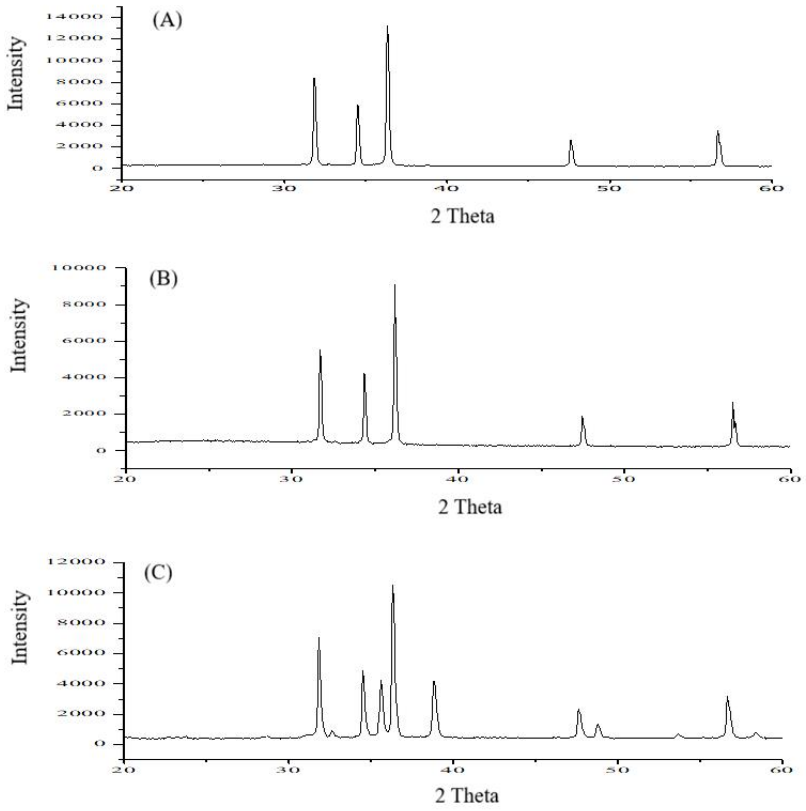

Figure 2. XRD patterns of Cu-d-ZnO NPs, prepared using (A) 1%, (B) 3%, and (C) 5% Cu concentrations.

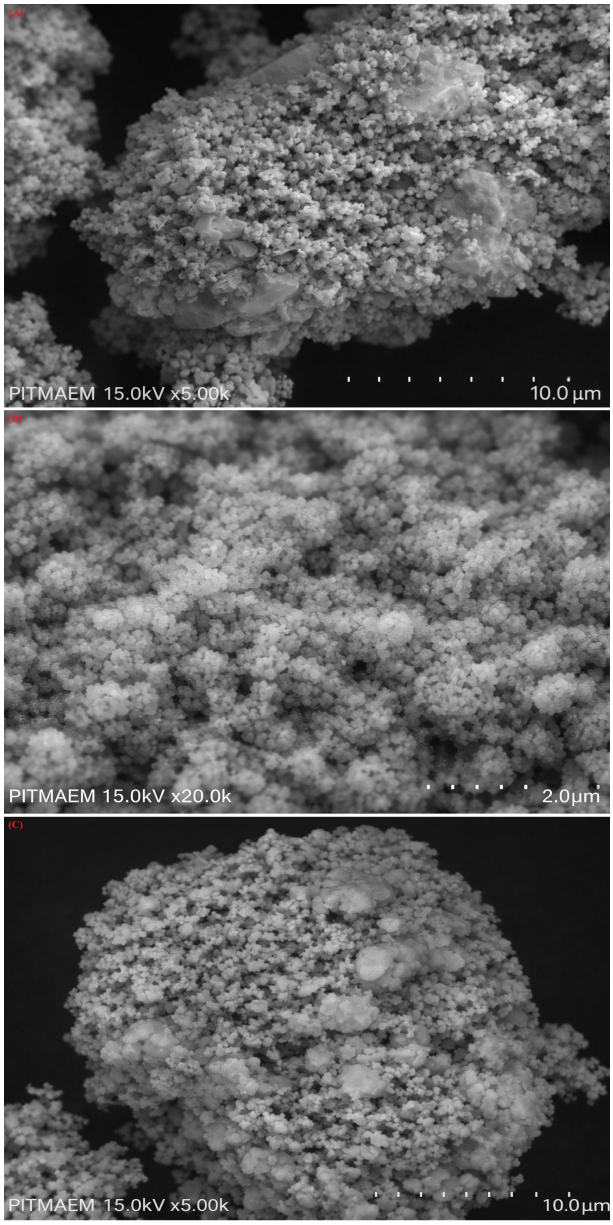

Figure 3. SEM images of Cu-d-ZnO NPs showing surface morphology and agglomeration, (A) 1 %, (B) 3 % and (C) 5 % Cu concentrations.

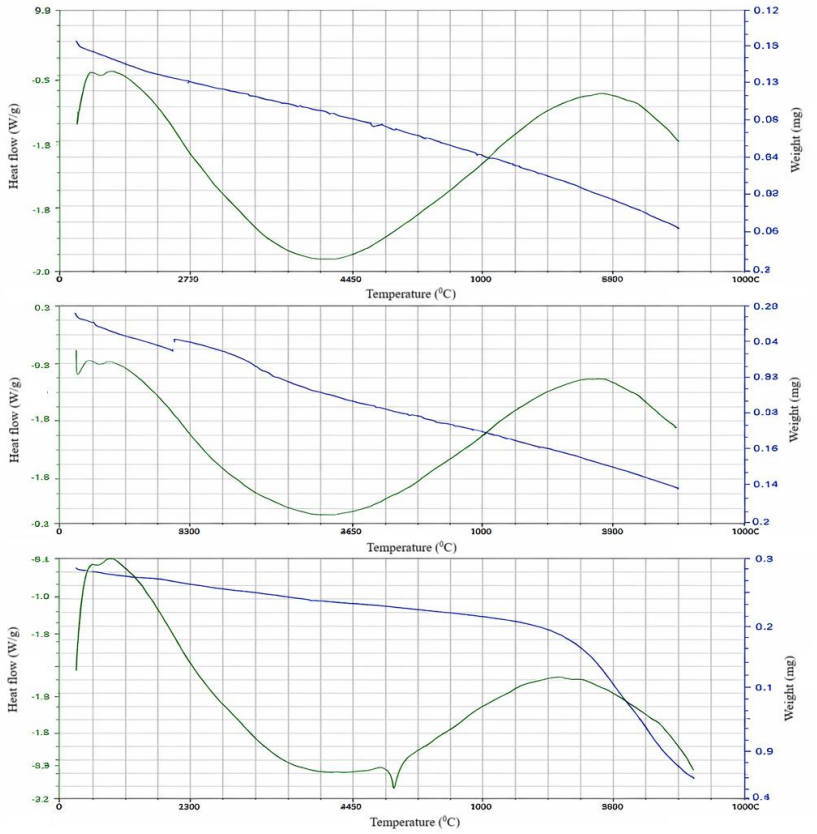

Figure 4. TG–DSC profiles of the Cu-d-ZnO NPs (Cu 1, 3 and 5% from top to bottom) recorded up to 1000 °C, illustrating weight loss and corresponding heat flow changes.

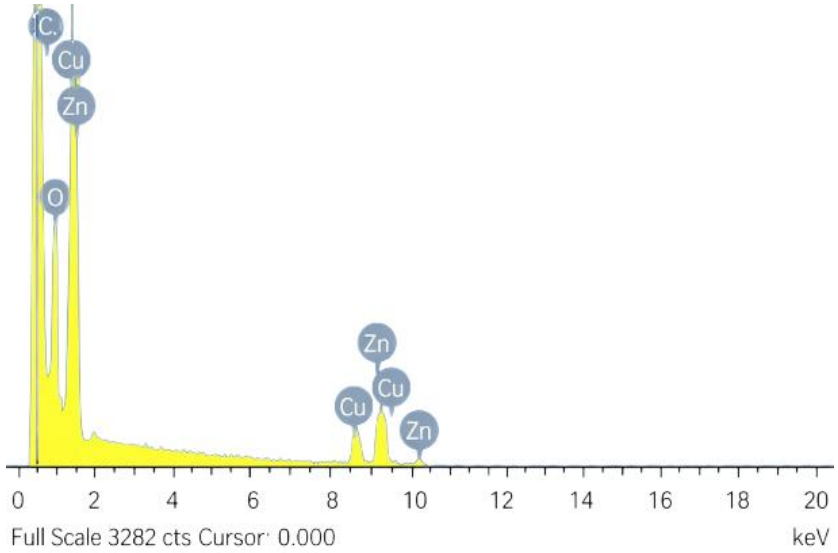

Figure 5. EDX spectrum of the 5%Cu-d-ZnO NPs showing characteristic peaks of Zn, Cu, O and C elements.

3.2. Photocatalytic activity

The Cu-d-ZnO and pure ZnO PCA were assessed for the MB dye. The Cu-d-ZnO PCA was higher versus ZnO for MB dye, however, doped ZnO showed higher efficiency (Fig. 6). The percentages degradation for ZnO, Cu(1%)-d-ZnO, Cu(3%)-d-ZnO and Cu(5%)-d-ZnO were 58, 70, 81 and 85.5 (%), respectively, which revealed that the Cu doping of ZnO enhanced the PCA and this enhanced PCA could be due to reactive species produced, i.e., $^{\bullet}OH/O_2^{\bullet-}$, which degraded the dye

through oxidative process and complex dye molecule is converted into low molecular species and finally, in to water and carbon dioxide [19]. The observations match well with already reported studies for PCA of ZnO and ZnO composites, i.e., NPE degradation under UV and solar illumination was studied and ZnO NPs showed promising efficiency as a photocatalyst under both types of lights [22]. Similarly, Ata et al. [23] studied the PCA of ZnO composite and found it highly active for dye degradation under UV light irradiation. These findings indicate that Cu-d-ZnO is an active catalyst for the degradation of dyes [24-27].

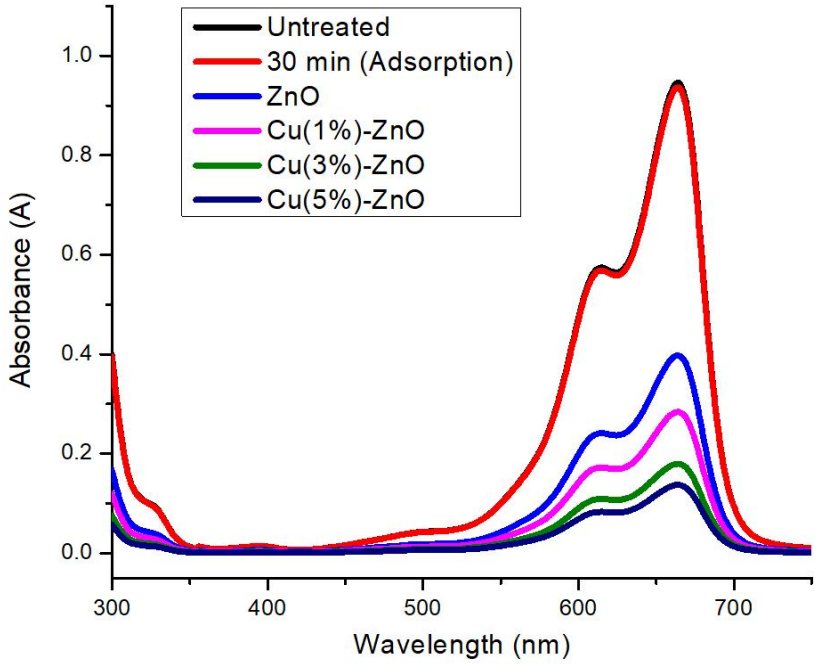

Figure 6. UV-visible spectra of untreated and treated MB dye using ZnO and Cu-d-ZnO under UV irradiation (120 min).

3.2.1. Photocatalytic activity mechanism

Cu-d-ZnO generates electron–hole pairs under photo-irradiation, where electrons are excited from the valence band (VB) to the conduction band (CB) upon absorption of photons (hν). The incorporated Cu^{2+} ions act as effective electron traps by capturing conduction-band electrons and being reduced to Cu^{+}, thereby suppressing electron–hole recombination and prolonging charge carrier lifetime. The photogenerated electrons in the CB react with dissolved oxygen to form superoxide radicals ($O_2^{\bullet-}$), while the photogenerated holes in the VB oxidize adsorbed water molecules or hydroxyl ions to generate hydroxyl radicals ($^{\bullet}OH$). Subsequently, $O_2^{\bullet-}$ reacts with protons (H^+) to form hydroperoxyl radicals ($HO_2^{\bullet}$), which further undergo disproportionation to produce H_2O_2. The generated H_2O_2 can be reduced by electrons to yield additional $^{\bullet}OH$ radicals. These processes collectively enhance the generation of reactive oxygen species (ROS), including $^{\bullet}OH$ and $O_2^{\bullet-}$, which are responsible for the degradation of organic pollutants. Furthermore, Cu doping introduces defect sites and oxygen vacancies that facilitate charge transfer and ROS formation. The synergistic effect of ZnO photoexcitation and Cu-induced electron trapping significantly enhances photocatalytic efficiency. As illustrated in Fig. 7 and summarized in Eqs. (3–12), the generated ROS effectively degrade methylene blue into intermediate species, which are subsequently mineralized into CO_2 and H_2O.

$ZnO + h\nu \rightarrow e^{-}(CB) + h^{+}(VB)$ (3)

$Cu^{2+} + e^{-} \rightarrow Cu^{+}$ (acts as an electron trap and suppresses recombination) (4)

$e^{-}(CB) + O_2 \rightarrow O_2^{\bullet-}$ (5)

$h^{+}(VB) + H_2O \rightarrow H^{+} + {}^{\bullet}OH$ (6)

$h^+(VB) + OH^- \rightarrow {}^\bullet OH$ (7)

$H^+ + O_2^{\bullet-} \rightarrow HO_2^\bullet$ (8)

$2HO_2^\bullet \rightarrow H_2O_2 + O_2$ (9)

$e^- + H_2O_2 \rightarrow {}^\bullet OH + OH^-$ (10)

$MB + {}^\bullet OH/O_2^{\bullet-} \rightarrow$ intermediate products (11)

Intermediate products + $^\bullet OH/O_2^{\bullet-} \rightarrow$ low-molecular-weight products + $CO_2 + H_2O$ (12)

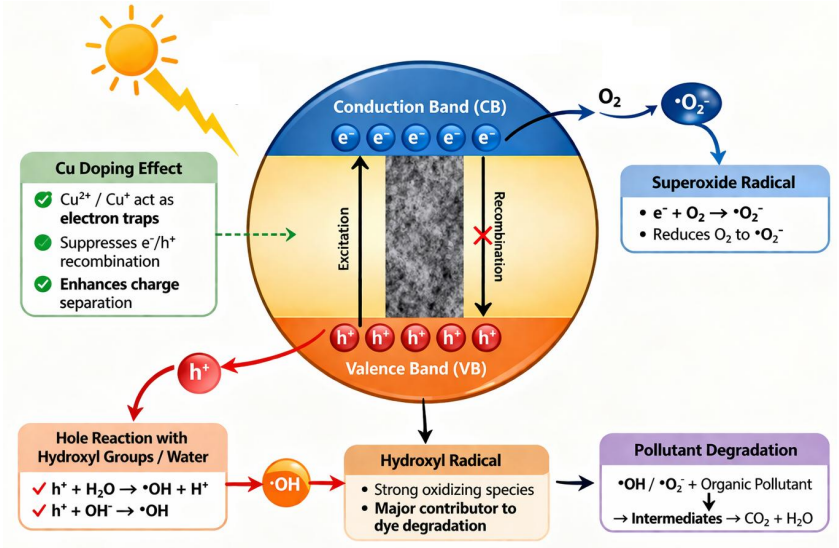

Figure 7. Proposed photocatalytic mechanism of pollutant (MB dye) using Cu-d-ZnO under UV light irradiation.

3.2.2. Scavenging studies

To identify the main active species involved in MB degradation and to gain deeper insight into the photocatalytic mechanism, reactive species trapping experiments were performed. Photogenerated electrons, holes, and hydroxyl radicals were selectively scavenged using $AgNO_3$, EDTA, and 2-propanol, respectively. Upon the addition of each scavenger (3 mM) under identical experimental conditions, a noticeable decrease in photocatalytic efficiency was observed (Fig. 8), confirming the involvement of multiple reactive species in the degradation process. Specifically, MB removal decreased from 85.5% (without scavenger) to 23.5% in the presence of $AgNO_3$, 53.5% with 2-propanol, and 78% with EDTA. The pronounced inhibition caused by $AgNO_3$ indicates that photogenerated electrons play a crucial role in the photocatalytic process. However, electrons are not the primary oxidizing species; rather, they contribute indirectly by reducing dissolved oxygen to generate superoxide radicals ($O_2^{\bullet-}$), which participate in subsequent oxidation reactions. The moderate suppression observed with 2-propanol confirms the significant involvement of hydroxyl radicals ($^\bullet OH$), while the relatively smaller effect of EDTA suggests a comparatively lesser, yet still important, contribution of holes. These findings indicate that the photocatalytic degradation proceeds via a synergistic mechanism involving both $^\bullet OH$ and $O_2^{\bullet-}$ reactive oxygen species. In the Cu-d-ZnO system, Cu acts as an efficient electron-trapping center, which enhances charge separation and prolongs electron lifetime, which facilitates increased formation of $O_2^{\bullet-}$ radicals.

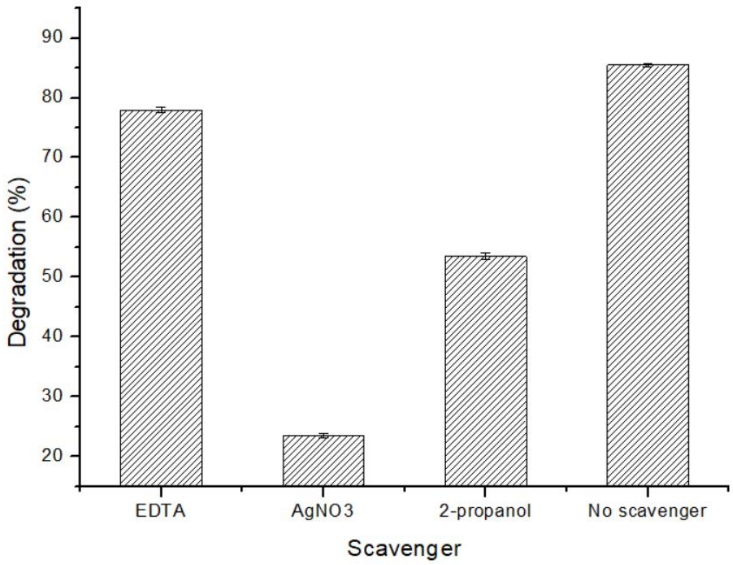

Figure 8. Scavenging studies for the identification of the species responsible for MB degradation in the presence of Cu-d-ZnO under UV light irradiation.

3.3. Antimicrobial activity

Antimicrobial activity of Cu-d-ZnO at different combinations of Cu such as (1-5%), was assessed against *B. subtilis, P. multocida, S. aureus* and *E. coli* bacterial strains, while *A. flavus, A. niger* and *P. notatum* were employed for antifungal activity evaluation (Fig. 9). Cu-d-ZnO showed promising antibacterial activity, which was higher against *S. aureus,* followed by *B. subtilis, P. multocida* and *E. coli.* The zone of inhibition was recorded in the range of 18±1.34 to 26±4.69 for *E. coli*, *P. multocida, and S. aureus.* The Cu-d-ZnO furnished up to 30% higher antimicrobial activity compared to pure ZnO. These observations matched well with already documented studies that ZnO nanodots are active microbial agents [33]. The ZnO and Cu-d-ZnO antifungal activity was low against the tested fungal strains. The zones of inhibition for fungal strains were in the 11-15 mm range and the standard drug (Fluconazole) showed the zones in the range of 27-29 mm. The MIC values were also estimated for bacterial and fungal strains (Fig. 10), which were in 178-354 μg/mL and 286-407 μg/mL in the case of bacterial strains and fungal strains, respectively. The MIC of the tested sample was 20 to 25% of Cu-d-ZnO versus pure ZnO, which is an indication that doping of Cu with ZnO enhanced the antimicrobial activity.

The antimicrobial activity of Cu-d-ZnO NPs was evaluated using the disc diffusion method, which provides qualitative to semi-quantitative information on the inhibitory potential against selected microbial strains. The results demonstrate that Cu incorporation enhances antibacterial activity compared to pristine ZnO, indicating that dopant modification improves the interaction between NPs and microbial strains. However, it should be noted that the disc diffusion method primarily reflects inhibition zone formation and does not provide a fully quantitative measure of antimicrobial potency. To support these observations, MIC values were determined, which showed trends consistent with the disc diffusion results. While these methods confirm enhanced antimicrobial performance, further quantitative assays would be required for a more comprehensive evaluation. The antibacterial mechanism is proposed based on established literature for metal-d-ZnO systems. The improved activity can be attributed to multiple factors, including enhanced generation of ROS, release of Cu^{2+} ions and direct interaction of NPs with microbial cell membranes. These effects can induce oxidative stress, disrupt membrane integrity and interfere with essential cellular functions, ultimately leading to cell damage. These results indicate that Cu doping improves the antimicrobial efficacy of ZnO NPs compared to the undoped counterpart.

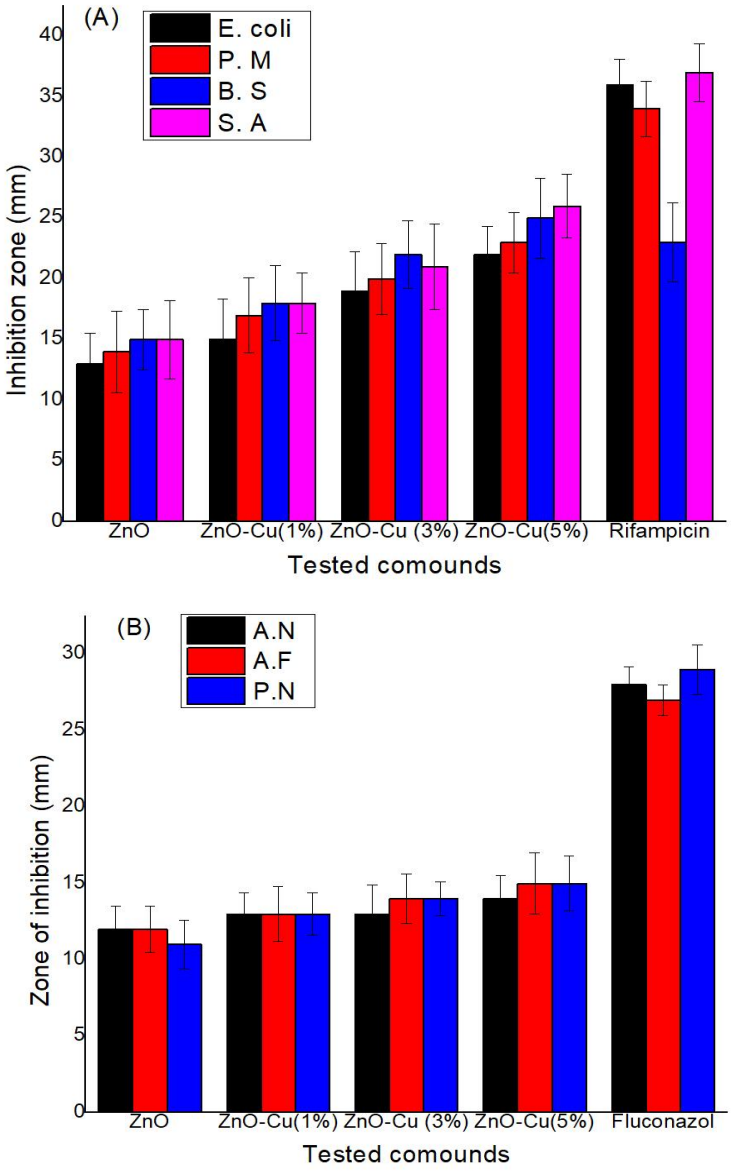

Figure 9. Antimicrobial activity (Zone of inhibition, mm) of ZnO and Cu-d-ZnO, (A) antibacterial activity and (B) antifungal activity.

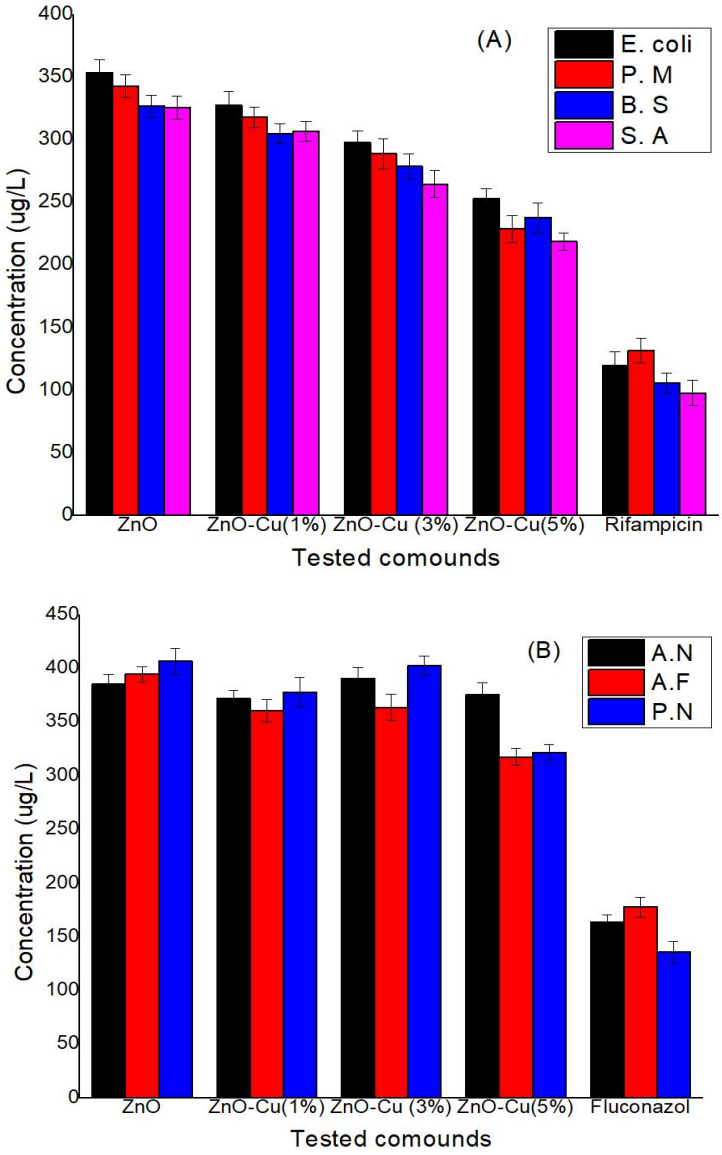

Figure 10. Antimicrobial activity (MIC, ug/mL) of ZnO and Cu-d-ZnO, (A) antibacterial and (B) antifungal.

4. Conclusions

Cu-d-ZnO NPs with Cu contents of 1–5 wt.% were successfully synthesized via a precipitation–dispersion method and characterized. XRD analysis confirmed the hexagonal wurtzite structure, with average crystallite sizes decreasing with increasing Cu content, indicating inhibition of crystal growth due to dopant incorporation. SEM analysis revealed agglomerated nanoscale clusters, while EDX confirmed the presence of Zn, O and Cu elements. Thermal analysis demonstrated good stability of the synthesized nanoparticles. Among the prepared samples, the 5 wt.% Cu-d-ZnO exhibited the highest photocatalytic activity, achieving 85.5% degradation of MB dye under UV light irradiation. This enhancement is attributed to improved charge separation and increased generation of ROS facilitated by Cu-induced defect states and electron-trapping behavior. Scavenger studies confirmed that both superoxide radicals ($O_2^{\bullet-}$) and hydroxyl radicals ($^{\bullet}OH$) are involved in the degradation process, indicating a synergistic reaction mechanism. Furthermore, antimicrobial studies showed enhanced antibacterial performance of Cu-d-ZnO NPs as compared to pristine ZnO, with MIC values ranging from 178–354 μg/mL. The improved activity is attributed to ROS generation, release of Cu^{2+} ions and interactions with microbial cell membranes, which requires further experimental validation.

The results demonstrate that Cu doping significantly improves the photocatalytic and antimicrobial performance of ZnO NPs, highlighting their potential for environmental remediation applications. Future work should focus on optimizing operational parameters, conducting detailed mechanistic studies, evaluating toxicity and environmental safety for practical applications.

Author Contributions: NA, MS, MI conceived and designed the research framework; NA, MSA carried out the experimental and computational work; MA, IB, AHA, NT provided critical guidance on the analytical methods and interpretation of results; NA, MA, AN performed the data analysis; NA, MSA, MI prepared the initial draft of the manuscript. All authors have read and approved the final manuscript. All authors contributed to editorial changes in the manuscript. All authors have participated sufficiently in the work and agreed to be accountable for all aspects of the work.

Acknowledgments: The authors extend their appreciation to the Deanship of Scientific Research and Libraries in Princess Nourah bint Abdulrahman University for funding this research work through the Research Group project, Grant No. (RG-1445-0041). The authors sincerely thank the anonymous reviewers for their valuable comments and constructive suggestions, which significantly improved the quality and clarity of the manuscript. The authors gratefully acknowledge Dr. Naveed Ahmad (University of Education) for his assistance with data analysis, which significantly contributed to the successful completion of this research.

Availability of Data and Materials: The datasets used and analyzed during the current study are available from the corresponding author on reasonable request.

Funding: The authors extend their appreciation to the Deanship of Scientific Research and Libraries in Princess Nourah bint Abdulrahman University for funding this research work through the Research Group project, Grant No. (RG-1445-0041).

Conflict of interest: The authors declare no conflict of interest.

References

1. Lia, Y.; Chen, X.; Wang, Z. Visible-light Z-scheme MoS_2/CdS heterostructure for photocatalytic degradation of organics and surfactants in produced water. *Journal of Ovonic Research* 2025, 21, 875-888. https://doi.org/10.15251/JOR.2025.216.875
2. Naseem, A.; Nadeem, N.; Noreen, S.; Youssef, M.; Rehan, Z.; Ali, H.; Mustafa, G.; Zahid, M. Sunlight-activated photocatalytic efficiency of novel Zr-CoS-PTh composite for superior wastewater remediation. *Journal of Ovonic Research* 2025, 21, 565-578. https://doi.org/10.15251/JOR.2025.215.565
3. Kalaivania, P.; Mathubala, G. The green combustion technique for synthesizing CuO nanoparticles with an extract from Azadirachta indica seeds: Potential anticancer and photocatalytic studies using organic dye. *Digest Journal of Nanomaterials and Biostructures* 2025, 20, 37-53. https://doi.org/10.15251/DJNB.2025.201.37
4. Timsorn, K.; Ellis, T.; Seekaew, Y.; Wongchoosuk, C. Metal/metal oxide nanoparticles decorated carbon nanomaterials-based gas sensors: A review. *Micro and Nanostructures* 2026, 209, 208406. https://doi.org/10.1016/j.micrna.2025.208406
5. Kavaz, D. Effective methylene dye removal from contaminated water using zinc oxide nanoparticles fabricated from the green synthesis of *Laurus nobilis* leaf. *Journal of the Chemical Society of Pakistan* 2024, 46, 535-549. https://doi.org/10.52568/001614/JCSP/46.06.2024
6. ul haq, I.; Khan, M.I.; Li, M.; Alshahrani, D.O.; Amami, M. Bandgap engineering and efficiency enhancement in Cs2AgBiBr6 solar cells through MAPbI2Br incorporation. *Materials Chemistry and Physics* 2026, 348, 131376. https://doi.org/10.1016/j.matchemphys.2025.131376
7. Sahay, P.; Nath, R. Al-doped zinc oxide thin films for liquid petroleum gas (LPG) sensors. *Sensors and Actuators B: Chemical* 2008, 133(1), 222-227. https://doi.org/10.1016/j.snb.2008.02.014
8. Bharathi, P.; Krishna Mohan, M.; Shalini, V.; Harish, S.; Navaneethan, M.; Archana, J.; Ganesh Kumar, M.; Dhivya, P.; Ponnusamy, S.; Shimomura, M.; Hayakawa, Y. Growth and influence of Gd doping on ZnO nanostructures for enhanced optical, structural properties and gas sensing

applications. *Applied Surface Science* 2000, 499, 143857. https://doi.org/10.1016/j.apsusc.2019.143857

9. Sikam, P.; Moontragoon, P.; Ikonic, Z.; Kaewmaraya, T.; Thongbai, P. The study of structural, morphological and optical properties of (Al, Ga)-doped ZnO: DFT and experimental approaches. *Applied Surface Science* 2019, 480, 621-635. https://doi.org/10.1016/j.apsusc.2019.02.255
10. Wang, J.; Shen, T.; Feng, Y.; Liu, H. A GGA+U study of electronic structure and the optical properties of different concentrations Tb doped ZnO. *Physica B: Condensed Matter* 2019, 411720. https://doi.org/10.1016/j.physb.2019.411720
11. Sankar Ganesh, R.; Patil, V.L.; Durgadevi, E.; Navaneethan, M.; Ponnusamy, S.; Muthamizhchelvan, C.; Kawasaki, S.; Patil, P.S.; Hayakawa, Y. Growth of Fe doped ZnO nanoellipsoids for selective NO2 gas sensing application. *Chemical Physics Letters* 2019, 734, 136725. https://doi.org/10.1016/j.cplett.2019.136725
12. Huang, X.; Li, C.; Qian, L.; Li, M.; Li, H.; Niu, X.; Yang, B. Improved ethanol vapor sensing properties of sputtered ZnO films by doping Ta. *Materials Today Communications* 2019, 21, 100680. https://doi.org/10.1016/j.mtcomm.2019.100680
13. Lee, Y.; Kim, S.; Jeong, S.Y.; Seo, S.; Kim, C.; Yoon, H.; Jang, H.W.; Lee, S. Surface-modified Co-doped ZnO photoanode for photoelectrochemical oxidation of glycerol. Catalysis Today 2019, 359, 43-49. https://doi.org/10.1016/j.cattod.2019.06.065
14. Guo, T.; Tan, S.; Xu, G.; Ma, J.; Liu, X.; Ji, G.; Liu, G.; He, Y.; Zhang, S. Temperature-dependent infrared emissivity property of Ce-doped ZnO nanoparticles. *Ceramics International* 2019, 46(2), 1569-1576. https://doi.org/10.1016/j.ceramint.2019.09.125
15. Khan, A.u.R.; Ramzan, M.; Khan, S.u.R.; Abid, I.; Binhuday, F.S.; Majid, M.A.; Rehman, A.; Singh, A. Sol-gel synthesis, characterizations of efficient Y^{3+} doped ZnO nanoparticles for photocatalytic dye degradation and energy storage applications. *Journal of Sol-Gel Science Technology* 2025, 113, 180-196. https://doi.org/10.1007/s10971-024-06597-1
16. Zhu, C.; Wang, X. Nanomaterial ZnO synthesis and its photocatalytic applications: A review. *Nanomaterials* 2025, 15(9), 682. https://doi.org/10.3390/nano15090682
17. Gindose, T.G.; Zereffa, E.A.; Atisme, T.B.; Sani, T.; Hailegebreal, T.D. A review on metal-doped zinc oxide–based single and multiple phase mixed oxide nanomaterials for photocatalytic applications. *Advances in Materials Science Engineering* 2025, 9925834. https://doi.org/10.1155/amse/9925834
18. Hashim, F.S.; Alkaim, A.F.; Salim, S.J.; Alkhayatt, A.H.O. Effect of (Ag, Pd) doping on structural, and optical properties of ZnO nanoparticales: As a model of photocatalytic activity for water pollution treatment. *Chemical Physics Letters* 2019, 737, 136828. https://doi.org/10.1016/j.cplett.2019.136828
19. Kokab, M.; Bibi, I.; Majid, F.; Kamal, S.; Taj, B.; Fatima, G.; Raza, Q.; Lim, S.; Alzahrani, F.M.; Nazir, A.; Iqbal, M. Solar light-based photocatalysis for organic pollutant degradation: Mechanistic understanding of double Z-scheme dynamics in ZnO/Fe_2O_3-doped $NiCo_2O_4$. *Solar Energy* 2025, 295， 113519. https://doi.org/10.1016/j.solener.2025.113519
20. Riaz, M.; Rasool, N.; Bukhari, I.; Shahid, M.; Zubair, M.; Rizwan, K.; Rashid, U. In vitro antimicrobial, antioxidant, cytotoxicity and GC-MS analysis of Mazus goodenifolius. Molecules, 17, 14275-14287. https://doi.org/10.3390/molecules171214275
21. Sarker, S.D.; Nahar, L.; Kumarasamy, Y. Microtitre plate-based antibacterial assay incorporating resazurin as an indicator of cell growth, and its application in the in vitro antibacterial screening of phytochemicals. *Methods* 2007, 42, 321-324. https://doi.org/10.1016/j.ymeth.2007.01.006
22. Ashar, A.; Iqbal, M.; Bhatti, I.A.; Ahmad, M.Z.; Qureshi, K.; Nisar, J.; Bukhari, I.H. Synthesis, characterization and photocatalytic activity of ZnO flower and pseudo-sphere: Nonylphenol ethoxylate degradation under UV and solar irradiation. *Journal of Alloys and Compounds* 2016, 678, 126-136. https://doi.org/10.1016/j.jallcom.2016.03.251
23. Ata, S.; Shaheen, I.; Ghafoor, S.; Sultan, M.; Majid, F.; Bibi, I.; Iqbal, M. Graphene and silver

decorated ZnO composite synthesis, characterization and photocatalytic activity evaluation. *Diamond and Related Materials* 2018, 90, 26-31. https://doi.org/10.1016/j.diamond.2018.09.015

24. Iqbal, Z.; Imran, M.; Latif, S.; Nazir, A.; Ibrahim, S.M.; Ahmad, I.; Iqbal, M.; Iqbal, S. Photocatalytic degradation of dyes in aqueous media by gum shellac stabilized selenium nanoparticles. *Zeitschrift für Physikalische Chemie* 2023, 237, 1139-1152. https://doi.org/10.1515/zpch-2022-0113
25. Nazir, A.; Zahid, S.; Mahmood, Z.; Kanwal, F.; Latif, S.; Imran, M.; Hassan, F.; Iqbal, M. Adsorption kinetics for the removal of toxic Congo red dye by polyaniline and citrus leaves as effective adsorbents. *Zeitschrift für Physikalische Chemie* 2022, 236, 1301-1319. https://doi.org/10.1515/zpch-2022-0014
26. Aslam, A.; Bhatti, H.N.; Fatima, S.; Ain, H.; Bibi, S.; Ibrahim, S.M.; Iqbal, M. Kinetics of acid blue 40 dye degradation under solar light in the presence of CuO nanoparticles synthesized using Citrullus lanatus seeds extract. *Zeitschrift für Physikalische Chemie* 2022, 236, 583-594. https://doi.org/10.1515/zpch-2021-3076
27. Kausar, A.; Naeem, K.; Iqbal, M.; Nazli, Z.-i.-H.; Bhatti, H.N.; Ashraf, A.; Nazir, A.; Kusuma, H.S.; Khan, M.I. Kinetics, equilibrium and thermodynamics of dyes adsorption onto modified chitosan: A review. *Zeitschrift für Physikalische Chemie* 2021, 235(11), 1499-1538. https://doi.org/10.1515/zpc-2019-1586
28. Al Abri, R.; Al Marzouqi, F.; Kuvarega, A.T.; Meetani, M.A.; Al Kindy, S.M.Z.; Karthikeyan, S.; Kim, Y.; Selvaraj, R. Nanostructured cerium-doped ZnO for photocatalytic degradation of pharmaceuticals in aqueous solution. *Journal of Photochemistry and Photobiology A: Chemistry* 2019, 384, 112065. https://doi.org/10.1016/j.jphotochem.2019.112065
29. Qi, K.; Xing, X.; Zada, A.; Li, M.; Wang, Q.; Liu, S.-y.; Lin, H.; Wang, G. Transition metal doped ZnO nanoparticles with enhanced photocatalytic and antibacterial performances: Experimental and DFT studies. *Ceramics International* 2019, 46(2), 1494-1502. https://doi.org/10.1016/j.ceramint.2019.09.116
30. Poornaprakash, B.; Chalapathi, U.; Subramanyam, K.; Vattikuti, S.V.P.; Park, S.-H. Wurtzite phase Co-doped ZnO nanorods: Morphological, structural, optical, magnetic, and enhanced photocatalytic characteristics. *Ceramics International* 2019, 46(3), 2931-2939. https://doi.org/10.1016/j.ceramint.2019.09.289
31. Rath, P.P.; Behera, S.S.; Priyadarshini, B.; Panda, S.R.; Mandal, D.; Sahoo, T.; Mishra, S.; Sahoo, T.R.; Parhi, P.K. Influence of Mg doping on ZnO NPs for enhanced adsorption activity of Congo Red dye. *Applied Surface Science* 2019, 491, 256-266. https://doi.org/10.1016/j.apsusc.2019.06.120
32. Ramos-Corona, A.; Rangel, R.; Alvarado-Gil, J.J.; Bartolo-Pérez, P.; Quintana, P.; Rodríguez-Gattorno, G. Photocatalytic performance of nitrogen doped ZnO structures supported on graphene oxide for MB degradation. *Chemosphere* 2019, 236, 124368. https://doi.org/10.1016/j.chemosphere.2019.124368
33. Duan, G.; Chen, L.; Jing, Z.; De Luna, P.; Wen, L.; Zhang, L.; Zhao, L.; Xu, J.; Li, Z.; Yang, Z. Robust antibacterial activity of tungsten oxide (WO_{3-X}) nanodots. *Chemical Research in Toxicology* 2019, 32, 1357-1366. https://doi.org/10.1021/acs.chemrestox.8b00399
34. Prabavathi, N.; Mary, S.S.; Dhanavel, S. Unravelling the potential of ZnO and Cu-doped ZnO nanoparticles for photocatalytic degradation of organic dyes and antimicrobial applications. *Research on Chemical Intermediates* 2025, 52, 1117-1146. https://doi.org/10.1007/s11164-025-05857-1 (2025) 1-30